Published in final edited form as:
Nat Methods. ; 9(3): 263–265. doi:10.1038/nmeth.1867.

Lipidic phase membrane protein serial femtosecond crystallography

Linda C Johansson[1], **David Arnlund**[1], **Thomas A White**[2], **Gergely Katona**[1], **Daniel P DePonte**[2], **Uwe Weierstall**[3], **R Bruce Doak**[3], **Robert L Shoeman**[4], **Lukas Lomb**[4], **Erik Malmerberg**[1], **Jan Davidsson**[5], **Karol Nass**[6], **Mengning Liang**[2], **Jakob Andreasson**[7], **Andrew Aquila**[2,8], **Sasa Bajt**[8], **Miriam Barthelmess**[8], **Anton Barty**[2], **Michael J Bogan**[9], **Christoph Bostedt**[10], **John D Bozek**[10], **Carl Caleman**[2], **Ryan Coffee**[10], **Nicola Coppola**[2,18], **Tomas Ekeberg**[7], **Sascha W Epp**[11,12], **Benjamin Erk**[11,12], **Holger Fleckenstein**[2], **Lutz Foucar**[4,11], **Heinz Graafsma**[8], **Lars Gumprecht**[2], **Janos Hajdu**[7], **Christina Y Hampton**[9], **Robert Hartmann**[13], **Andreas Hartmann**[13], **Günter Hauser**[14,15], **Helmut Hirsemann**[8], **Peter Holl**[13], **Mark S Hunter**[16], **Stephan Kassemeyer**[4], **Nils Kimmel**[14,15], **Richard A Kirian**[3], **Filipe R N C Maia**[17], **Stefano Marchesini**[17], **Andrew V Martin**[2], **Christian Reich**[13], **Daniel Rolles**[4,11], **Benedikt Rudek**[11,12], **Artem Rudenko**[11,12], **Ilme Schlichting**[4,11], **Joachim Schulz**[2], **M Marvin Seibert**[7,18], **Raymond G Sierra**[9], **Heike Soltau**[13], **Dmitri Starodub**[9], **Francesco Stellato**[2], **Stephan Stern**[2], **Lothar Strüder**[14,15], **Nicusor Timneanu**[7], **Joachim Ullrich**[11,12], **Weixiao Y Wahlgren**[1], **Xiaoyu Wang**[3], **Georg Weidenspointner**[14,15], **Cornelia Wunderer**[8], **Petra Fromme**[16], **Henry N Chapman**[2,6], **John C H Spence**[3], and **Richard Neutze**[1]

[1]Department of Chemistry and Molecular Biology, University of Gothenburg, Gothenburg, Sweden

[2]Center for Free-Electron Laser Science, Deutsches Elektronen-Synchrotron, Hamburg, Germany

[3]Department of Physics, Arizona State University, Tempe, Arizona, USA

[4]Max-Planck-Institut für Medizinische Forschung, Heidelberg, Germany

[5]Department of Photochemistry and Molecular Science, Uppsala University, Uppsala, Sweden

[6]Institute for Experimental Physics, University of Hamburg, Hamburg, Germany

[7]Laboratory of Molecular Biophysics, Department of Cell and Molecular Biology, Uppsala University, Uppsala, Sweden

Correspondence should be addressed to R.N. (richard.neutze@chem.gu.se)..
[18]Present addresses: European XFEL GmbH, Hamburg, Germany (N.C.) and Linac Coherent Light Source, SLAC National Accelerator Laboratory, Menlo Park, California, USA (M.M.S.).

Accession codes. Protein Data Bank: 4ac5.

Note: Supplementary information is available on the Nature Methods website.

AUTHOR CONTRIBUTIONS

L.C.J., R.N., H.N.C., J.C.H.S. and P.F. conceived the experiment, which was designed with A.B., R.A.K., J.C.H.S., D.P.D., U.W., R.B.D., M.J.B., D.S., I.S., S.M. and J.H. S.W.E., R.H., D.R., A.R., L.F., N.K., P.H., B.R., B.E., A.H., C.R., G.W., L.S., G.H., H.G., J.U., I.S., H.S., M.B., H.H., L.G. and H.G. designed and set up the CAMP instrument and/or developed and operated the pnCCD detectors. C.B. and J.D.B. set up and aligned the beamline; L.C.J. and D.A. grew sponge phase crystals; U.W., R.B.D., J.C.H.S., D.P.D., R.L.S. and L.L. designed and operated the injector; H.N.C., A.B., A.A., J.S., D.P.D., U.W., R.B.D., S.B., M.J.B., L.G., J.H., M.M.S., N.T., J.A., S.S. and J.C.H.S. developed diffraction instrumentation; L.C.J., D.A., T.A.W., D.P.D., U.W., R.B.D., R.L.S., L.L., E.M., J.D., K.N., M.L., A.A., M.B., A.B., M.J.B., C.B., J.D.B., C.C., R.C., N.C., T.E., H.F., P.F., C.Y.H., M.S.H., S.K., R.A.K., F.R.N.C.M., A.V.M., I.S., M.M.S., R.G.S., F.S., N.T., X.W., C.W., H.N.C., J.C.H.S. and R.N. collected data; L.C.J., D.A., T.A.W., G.K., W.Y.W. and K.N. analyzed the diffraction data using software developed by J.C.H.S., T.A.W., R.A.K., A.B. and H.N.C.; L.C.J. and R.N. wrote the paper with discussion and improvements from all authors.

COMPETING FINANCIAL INTERESTS

The authors declare no competing financial interests.

[8]Photon Science, Deutsches Elektronen-Synchrotron, Hamburg, Germany

[9]Photon Ultrafast Laser Science and Engineering Center Institute, Stanford Linear Accelerator Center (SLAC) National Accelerator Laboratory, Menlo Park, California, USA

[10]Linac Coherent Light Source, SLAC National Accelerator Laboratory, Menlo Park, California, USA

[11]Max Planck Advanced Study Group, Center for Free-Electron Laser Science, Hamburg, Germany

[12]Max-Planck-Institut für Kernphysik, Heidelberg, Germany

[13]PNSensor GmbH, München, Germany

[14]Max-Planck-Institut Halbleiterlabor, München, Germany

[15]Max-Planck-Institut für extraterrestrische Physik, Garching, Germany

[16]Department of Chemistry and Biochemistry, Arizona State University, Tempe, Arizona, USA

[17]Advanced Light Source, Lawrence Berkeley National Laboratory, Berkeley, California, USA

Abstract

X-ray free electron laser (X-feL)-based serial femtosecond crystallography is an emerging method with potential to rapidly advance the challenging field of membrane protein structural biology. here we recorded interpretable diffraction data from micrometer-sized lipidic sponge phase crystals of the *Blastochloris viridis* photosynthetic reaction center delivered into an X-feL beam using a sponge phase micro-jet.

Studying membrane proteins remains a major challenge for structural biologists. These proteins contain hydrophobic and hydrophilic surfaces, are typically scarce and highly flexible, frequently become unstable when removed from their natural membrane environment and are usually difficult to grow into large, well-ordered crystals suitable for conventional crystallography. Serial femtosecond crystallography[1], which allows X-ray diffraction data to be recorded from thousands of sub-micrometer- to micrometer-sized crystals, holds great promise for the structural analysis of membrane proteins. This emerging method has been first demonstrated[1] using sub-micrometer crystals of cyanobacterial photosystem I (PSI) delivered to the X-ray beam using a thin liquid jet[2]. PSI, which is a large membrane protein complex, is exceptional in that it crystallizes overnight at low ionic strength[3] (8 mM $MgSO_4$). More representative membrane protein crystallization conditions involve higher concentrations of salt (typically 50-300 mM) and polyethylene glycol (PEG; typically 10-35%), which pose challenges for micro-jet injection owing to higher viscosity and the risk that salt crystals or aggregates may clog the micro jet nozzle.

Lipidic cubic phase (LCP) crystallization of membrane proteins[4-6] is a generic crystallization method developed to mimic the natural lipid bilayer of membrane proteins and thereby enhance their stability during crystallization. In the original formulation[4], solubilized membrane proteins were first mixed with the lipid monoolein in the ratio 60:40 to form the semisolid LCP, to which crystallization agents were then added. LCP crystallization rapidly led to X-ray structures of archaeal rhodopsins[6] and more recently structures of G protein-coupled receptors[7] (Supplementary Note and Supplementary Table 1).

Because of its semisolid nature, the LCP does not readily form a micrometer-sized jet required to deliver microcrystals in serial femtosecond crystallography[1]. In contrast, the

closely related lipidic sponge phase (LSP), made by mixing monoolein and water with a third agent such as jeffamine or PEG that swells the cubic phase into a liquid phase[6,8], can be adapted to serial femtosecond crystallography. LSP crystallization was originally developed from the observation that the LCP crystallization of the *Rhodobacter sphaeroides* reaction center proceeded via an LSP[8]. Four independent LSP membrane protein structures have been reported to date (Supplementary Table 1); it appears likely that crystals used for determining the structures of several G protein-coupled receptors and one bacterial oxidase grew via a cubic-to-sponge-phase transition (Supplementary Note), and an LSP crystallization screen gave leads from 8 of 11 membrane proteins tested[9]. In this work we adapted the LSP crystallization to yield showers of membrane protein microcrystals that we injected across an X-ray free electron beam using microjet technology[2]. From the diffraction data we recovered a new crystal form of the *Bl. viridis* photosynthetic reaction center (RC_{vir}) solved using serial femtosecond crystallography.

For batch LSP crystallization experiments we modified earlier hanging-drop conditions[10] (Online Methods): we dispensed 250 μl aliquots in septum-sealed glass vials (Fig. 1a). Because the sponge phase is less dense than water, it spontaneously separates[8], with the LSP floating on the top (Fig. 1a). We used optical microscopy to identify crystallization conditions under which showers of microcrystals grew in the LSP over 2 weeks (Fig. 1b) and used cross-polarization analysis to confirm their ordered nature through birefringence (Supplementary Fig. 1). We shipped these sealed glass vials at room temperature to the Linac Coherent Light Source (LCLS) at SLAC National Laboratory, USA. We collected the colored upper phase (Fig. 1a) and removed large crystals that could potentially block the micro-jet by passing the LSP through a 10-μm-cutoff metal filter (Online Methods and Supplementary Fig. 2). We injected these suspensions as a rapidly flowing liquid micro-jet[2] across a focused X-FEL beam[11]. The sponge phase (Fig. 1a) readily flowed at a rate similar to that of water (10 μl min^{-1}) and produced a stable jet ~4 μm in diameter (Fig. 2a). Because the diameter of this jet was of the same order of magnitude as that of the RC_{vir} microcrystals, the LSP provided a low-background environment for serial femtosecond crystallography.

We collected diffraction data at the Atomic Molecular and Optical (AMO) beamline[12] of the LCLS on the Center for Free-Electron Laser Science Advanced Study Group multipurpose chamber (CAMP) pn-junction charge-coupled devices[13] (pnCCDs) with two vertically offset panels that we read out at 60 Hz, which was the repetition rate of the FEL X-ray pulses. Each X-FEL pulse was nominally 70 fs in duration and contained up to 10^{13} 2-keV X-rays (6.17 Å wavelength) focused into a 10 μm^2 spot. The maximum resolution accessible with this energy and detector geometry was 7.4 Å, and reaction center microcrystals repeatedly diffracted to this resolution limit (Fig. 2b). Of the 365,035 recorded frames (~100 min of data collection), we observed 1,542 diffraction patterns of which we processed 265 in the space group $P2_12_12_1$ (Fig. 2c) with unit cell axes a = 57.6 Å, b = 84.6 Å, c = 375.8 Å and unit cell angles $\alpha = \beta = \gamma = 90°$ (Supplementary Fig. 3), representing a new crystal form of RC_{vir}.

As we processed 265 diffraction patterns from 365,035 images, the hit rate was below 0.1%, approximately an order of magnitude lower than that obtained for PSI[1]. A probable explanation for this difference is that the RC_{vir} microcrystals tended to have a high mosaic spread (Supplementary Fig. 4), which, in combination with one cell axis being longer than 300 Å, made data-processing challenging. Because we grew PSI microcrystals overnight on-site at the LCLS[1], it is reasonable to expect that the quality of RC_{vir} microcrystals would improve if long-distance shipping at room temperature could be avoided. Further improvements include more robust diffraction-spot finding and indexing routines and changes in crystallization conditions to maximize the number of diffracting microcrystals.

We processed these diffraction data using Monte Carlo methods[14,15] because each diffraction pattern recorded only partial reflections from randomly oriented microcrystals. We summarize the crystallographic data recovered from this analysis in Supplementary Table 2 and provide crystallographic statistics for each resolution shell in Supplementary Table 3. The best molecular replacement solution (Online Methods) showed the crystals to pack as stacked layers of 2D crystals typically found in lipidic phase crystallization[6] (Supplementary Fig. 5). During structural refinement we cut the diffraction data to 8.2 Å resolution for which the multiplicity was greater than 4 and completeness was above 95% (Supplementary Table 3). Structural refinement yielded crystallographic R factor R_{factor} and R_{free} values of 35% and 38%, respectively (Supplementary Table 2; in Supplementary Table 4 we provide a breakdown by resolution shell) and both the $2F_{\text{obs}}$ - F_{calc} (where F_{obs} and F_{calc} are the observed and calculated structure factor amplitudes) electron density map (Fig. 3a) and composite omit map (Supplementary Fig. 6) clearly indicated transmembrane α helices. Moreover, when we removed all four heme groups of the RC_{vir} cytochrome subunit from the structural model, we recovered positive F_{obs} - F_{calc} electron density associated with each of these cofactors in the resulting omit map (Fig. 3b and Supplementary Fig. 7).

We also recovered well-performing micro-jets using LSPs derived from monoolein, water and PEG 400, PEG 1500 or PEG 4000 (Supplementary Fig. 8). As jeffamine and PEG conditions form the basis of a validated LSP crystallization screen[9], and PEG 400 has been a crystallization agent in all recent LCP crystal structures of G-protein-coupled receptors (Supplementary Table 1), the adaption of LSP crystallization to serial femtosecond crystallography appears promising for solving membrane protein targets of unknown structure.

Shorter X-ray wavelength beamlines (λ of ~1.5 Å) and higher repetition rates (120 Hz) have recently become available at the LCLS. As such, high-resolution membrane protein crystal structures should soon be achievable using X-FEL radiation. We estimate that an order of 10,000 processed diffraction images will be needed for high-resolution electron density maps to be recovered using serial femtosecond crystallography, which would require three 12-h shifts at the hit rate reported here. Nevertheless, because we solved the structure of RC_{vir} to 8.2 Å resolution by molecular replacement with only 265 processed images, this bodes well for future applications of lipidic phase serial femtosecond crystallography to membrane protein structural biology.

ONLINE METHODS

Growth and purification of reaction center from *Bl. viridis*

We cultivated the photosynthetic reaction center from *Bl. viridis* as described[10]. We modified the purification by using 250 ml POROS ‘50 micron’ HQ media (Applied Biosystems Europe BV) packed in an XK 50/20 column (GE Healthcare) and a HiPrep 26/60 Sephacryl S-300 column (GE Healthcare). This protocol yielded ~3 mg of pure RC_{vir} per liter of cell culture.

Lipidic sponge phase batch crystallization

We prepared LSPs as previously described[10]. We set up batch crystallizations in septum-sealed glass vials (Sigma-Aldrich) containing 100 μl protein (20-30 mg ml^{-1}), 100 μl LSP (12% monoolein, 17.5% jeffamine M-600, 1.0 M Hepes (pH 8.0), 0.7 M $(NH_4)_2SO_4$ and 2.5% 1,2,3-heptanetriol) and 50 μl of 1.0-1.2 M trisodium citrate. These setups were left to equilibrate for 2-4 weeks at 20 °C. We diluted crystals 4:1 in a solution containing 0.1 M Hepes (pH 8.0), 0.1% lauryldimethylamine-oxide (LDAO) before filtering in a 10-μm-cutoff titanium filter (VICI AG International). We developed the conditions for large-batch

crystallization setups by initially screening for batch crystallization conditions using smaller batch crystallization volumes (60 μl to 100 μl setups).

Liquid microjet

We delivered samples to the injector nozzle via a sample loop, and we injected these into the X-FEL beam at a flow rate of 10 μl min^{-1}. The liquid capillary of the nozzle had an inner diameter of 50 μm and the liquid was focused by coaxially flowing helium gas to a continuous jet-stream of ~4 μm diameter[2]. We aligned the X-ray beam to hit the liquid in the continuous jet region before the breakup into droplets occurred (Fig. 2a). For PEG-based LSPs, we required an inner diameter of 100 μm for the jet to flow (Supplementary Fig. 8). These LSPs consisted of 40% PEG 400, PEG 1500 or PEG 4000 mixed with 30% Monoolein and 30% buffer (0.1 M Hepes, pH 8.0, 0.1 M NaCl and 0.1 M $MgCl_2$).

Data collection

We collected diffraction data at the atomic molecular and optical (AMO) beamline at the Linac Coherent Light Source[12] using the CAMP instrument[13]. We recorded diffraction data on two 76.8 mm by 38.4 mm pnCCDs located 64.7 mm and 67.7 mm from the sample position. The pnCCDs we offset asymmetrically such that X-ray diffraction was sampled from 3.5° to 49.0°, which maximized the sampled resolution (7.4 Å at the outer corners; Fig. 2b). The X-ray wavelength at AMO was 6.17 Å, and we focused the beam to a 10 μm^2 spot.

Data processing

We processed diffraction data using in-house code that called DirAx[16] and MOSFLM[17] for automated indexing[1]. We indexed data from 265 diffraction images in $P2_12_12_1$ with unit cell axes a = 57.6 Å, b = 84.6 Å, c = 375.8 Å and $\alpha = \beta = \gamma = 90°$. We did not observe subpopulations of other crystal forms (Supplementary Fig. 3). Small variations in the length of the c axis, however, arose perhaps owing to pulse-to-pulse fluctuations in the X-FEL wavelength. Because every observation is a partial reflection, we scaled and merged this integrated data using Monte Carlo methods[14,15]. We estimated I/σ values for each resolution bin (Supplementary Table 3) from reflections with both positive intensity and a multiplicity higher than 1. NZ-test and L-test plots showed the expected distributions (Supplementary Fig. 9).

Molecular replacement and refinement

We obtained phases by molecular replacement using Phaser[18] 2.3.0 with PDB entry 2WJN[10] as the search model. The best solution had a translation function Z score (TFZ) of 8.5, the rotation function Z score (RFZ) of 5.8 and a log likelihood gain (LLG) of 81. This was well discriminated from second best solution with scores of TFZ, 4.6; RFZ, 5.8; and LLG, 39. We evaluated the crystal packing and confirmed that only the best molecular replacement solution was physically meaningful. We performed 20 cycles of rigid body and restrained refinement using REFMAC[19], converging to R_{factor} = 35% and R_{free} = 38%, and an overall figure of merit of 0.62. During refinement we used simple Wilson scaling and a constant density (using default values) we assigned to the region of the unit cell not occupied by protein atoms. We calculated the solvent mask using default parameters: increase van der Waals radius of non-ion atoms by 1.2 Å, increase ionic radius of potential ions by 0.8 Å, shrink the area of the mask by 0.8 Å after calculation. Crystallographic data statistics are summarized in Supplementary Table 2, and resolution shell breakdowns of the crystallographic data and refinement statistics are given in Supplementary Tables 3 and 4, respectively.

Control map calculations

We performed test calculations using two control datasets: one with the serial femtosecond crystallography data randomly shuffled and another where all observations were set equal. Molecular replacement failed with both control datasets. When we combined the phases generated using the molecular replacement solution recovered against the experimental data with these control datasets, the resulting electron density maps did not show α-helical structure (Supplementary Fig. 10).

Omit map calculations

We calculated F^{obs} - F^{calc} omit electron density maps using REFMAC[19] with all four hemes of the cytochrome subunit removed from the structural model (Fig. 3b and Supplementary Fig. 7).

Composite omit map calculations

We calculated composite omit electron density maps (Supplementary Fig. 6) using the program CNS[20,21] version 1.3 with ~5% of the structure excluded, no simulated annealing, no minimization and no bulk-solvent correction.

Supplementary Material

Refer to Web version on PubMed Central for supplementary material.

Acknowledgments

Experiments were carried out at the LCLS, a national user facility operated by Stanford University on behalf of the US Department of Energy, Office of Basic Energy Sciences. We acknowledge financial support from the Swedish Research Council (Vetenskapsrådet), the Swedish Foundation for International Cooperation in Research and Higher Education, Stiftelsen Olle Engkvist Byggmästare, the Max Planck Society for funding the development and operation of the CAMP instrument, the US National Science Foundation grant MCB 0919195, the US Department of Energy Office of Basic Energy Sciences through the Photon Ultrafast Laser Science and Engineering Center Institute at the SLAC National Accelerator Laboratory and the Energy Frontier Research Center for Bio-Inspired Solar Fuel Production (award DE-SC0001016), the Hamburg Ministry of Science and Research and Joachim Herz Stiftung as part of the Hamburg Initiative for Excellence in Research and the Hamburg School for Structure and Dynamics in Infection, US National Science Foundation (awards 0417142 and MCB-1021557), US National Institutes of Health (awards 1R01GM095583-01 and 1U54GM094625-01), the Deutsche Forschungsgemeinschaft Cluster of Excellence at the Munich Center for Advanced Photonics, Center for Biophotonics Science and Technology at the University of California (cooperative agreement PHY 0120999).

References

1. Chapman HN, et al. Nature. 2011; 470:73–77. [PubMed: 21293373]
2. DePonte DP, et al. J. Phys. D Appl. Phys. 2008; 41:195505.
3. Jordan P, et al. Nature. 2001; 411:909–917. [PubMed: 11418848]
4. Landau EM, Rosenbusch JP. Proc. Natl. Acad. Sci. USA. 1996; 93:14532–14535. [PubMed: 8962086]
5. Caffrey M. Annu. Rev. Biophys. 2009; 38:29–51. [PubMed: 19086821]
6. Johansson LC, Wöhri AB, Katona G, Engstrom S, Neutze R. Curr. Opin. Struct. Biol. 2009; 19:372–378. [PubMed: 19581080]
7. Rosenbaum DM, Rasmussen SG, Kobilka BK. Nature. 2009; 459:356–363. [PubMed: 19458711]
8. Wadsten P, et al. J. Mol. Biol. 2006; 364:44–53. [PubMed: 17005199]
9. Wöhri AB, et al. Structure. 2008; 16:1003–1009. [PubMed: 18611373]
10. Wöhri AB, et al. Biochemistry. 2009; 48:9831–9838. [PubMed: 19743880]
11. Emma P, et al. Nat. Photonics. 2010; 4:641–647.
12. Bozek JD. Eur. Phys. J. Spec. Top. 2009; 169:129–132.

13. Strüder L, et al. Nucl. Instrum. Methods Phys. Res. A. 2010; 614:483–496.
14. Kirian RA, et al. Opt. Express. 2010; 18:5713–5723. [PubMed: 20389587]
15. Kirian RA, et al. Acta Crystallogr. A. 2011; 67:131–140. [PubMed: 21325716]
16. Duisenberg AJ. J. Appl. Cryst. 1992; 25:92–96.
17. Leslie AGW. Acta Crystallogr. D. Biol. Crystallogr. 2006; 62:48–57. [PubMed: 16369093]
18. McCoy AJ, et al. J. Appl. Cryst. 2007; 40:658–674. [PubMed: 19461840]
19. Murshudov GN, Vagin AA, Dodson EJ. Acta Crystallogr. 1997; d53:240–255.
20. Brunger AT, et al. Acta Crystallogr. D Biol. Crystallogr. 1998; 54:905–921. [PubMed: 9757107]
21. Brunger AT. Nat. Protoc. 2007; 2:2728–2733. [PubMed: 18007608]

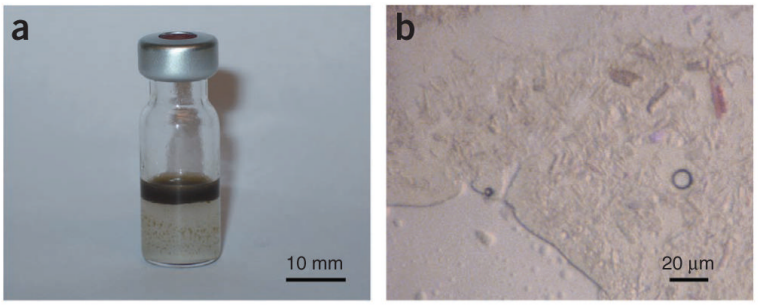

Figure 1.
LSP batch crystallization of RC_{vir}. (**a**) A 250-µl batch-crystallization setup in a glass vial with the sponge phase containing RC_{vir} (brown) floating on top. (**b**) Optical microscopy image of the sponge phase showing crystals. Larger crystals are ~20 µm long.

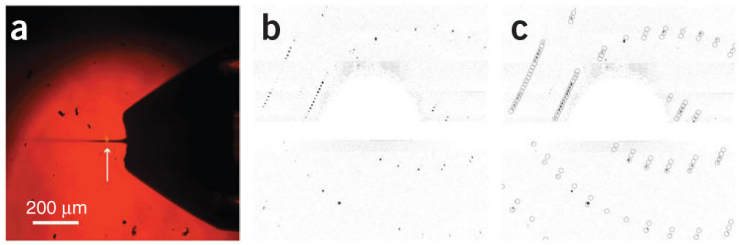

Figure 2.

Serial femtosecond crystallography of RC_{vir} crystals grown in a LSP. (**a**) Liquid jet formed by the sponge phase containing RC_{vir} crystals. The X-FEL beam interacting with the liquid jet is visible as a white fluorescent spot (white arrow). (**b**) Bragg diffraction spots (dark spots) recorded from a single RC_{vir} crystal using a single X-FEL pulse of 70 fs. (**c**) An identical diffraction image as shown in **b** but with the predicted spot positions after data indexing shown as circles. The resolution was limited to 7.4 Å in the corners of the lower pnCCD detector panel.

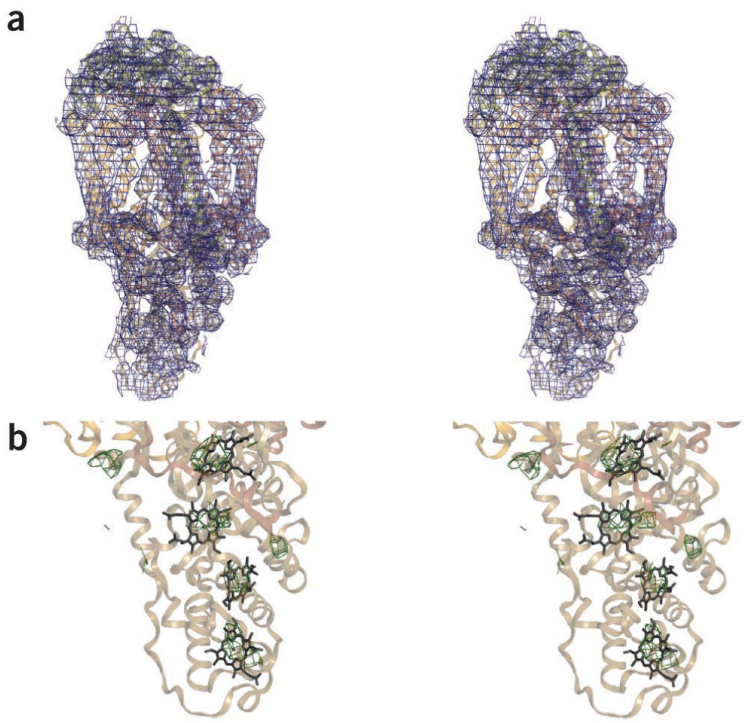

Figure 3.

Electron density for the LSP serial femtosecond crystallography RC$_{vir}$ structure at 8.2 Å resolution. (**a**) Stereo view of the 2m F_{obs} - DF_{calc} electron density map where m is the figure of merit and D is estimated from coordinate errors (contoured at 1.0 σ) recovered from 265 processed RC$_{vir}$ diffraction images. (**b**) Stereo view of the mF_{obs} - DF_{calc} omit electron density map (contoured at 2.0 σ), calculated with the four heme groups of the cytochrome subunit removed from the structural model. This figure was generated with Pymol (DeLano Scientific LLC).